RESEARCH PAPER

Application of CuFe₂O₄ Nanoparticles as an Effective Nanocarrier in Antibacterial Efficacy of Smart Drug Delivery System for Encapsulation of Gentamycin and Chloramphenicol

Mohinur Rabiyeva ^{1*}, Farrukh Namozov ¹, Dilnoza Karshieva ², Kamola Sattarova ³, Xosiyat Sanoyeva ⁴, Mahbuba Ziyayeva ⁵, Ravshan Abduraxmanov ⁶, Dilfuza Shodiyarova ⁷, Mukhabbat Buriyeva ⁸, Sherjon Sherjonov ⁹, Bunyod Kendjaev ¹⁰, Abdieva Nargiza Shukhratovna ¹¹, Abrorbek Samandarov ¹²

- ¹ Bukhara State Medical Institute named after Abu Ali ibn Sino, Bukhara, Uzbekistan
- ² Samarkand Campus, University of Economics and Pedagogy, Uzbekistan
- ³ Tashkent State Medical University, Tashkent, Uzbekistan
- ⁴ Bukhara State University, Bukhara, Uzbekistan
- ⁵ Jizzakh Polytechnic Institute, Jizzakh, Uzbekistan
- ⁶ Jizzakh Branch of the National University of Uzbekistan, Jizzakh, Uzbekistan
- ⁷ Samarkand State Medical University, Samarkand, Uzbekistan
- ⁸ Bukhara State Pedagogical Institute, Bukhara, Uzbekistan
- ⁹ Mamun University, Khorezm, Uzbekistan
- ¹⁰ Urganch Innovation University, Urgench, Uzbekistan
- ¹¹ Tashkent State University of Economics, Tashkent, Uzbekistan
- ¹² Urgench State University, Khorezm, Uzbekistan

ARTICLE INFO

$Article\ History:$

Received 26 June 2025 Accepted 28 September 2025 Published 01 October 2025

Keywords:

Antibacterial

 $CuFe_2O_4$

Nanocarrier

Nanoparticles

Gentamycin

Smart drug delivery system

ABSTRACT

Super-paramagnetic CuFe₂O₄ (18 ± 3 nm, 39 emu g⁻¹) was synthesised via CTAB-directed co-precipitation; antibiotics were surface-loaded under mild aqueous conditions to yield GT@CuFe₂O₄ (17.3 wt % gentamycin) and CM@CuFe2O4 (9.1 wt % chloramphenicol). Bactericidal activity was quantified by broth micro-dilution and drop-plate enumeration against ATCC 25922 and 29213 strains; magnetic guidance (1.3 T) and release kinetics (pH 5.5/7.4) were monitored by ICP-OES and HPLC-UV. GT@ CuFe₂O₄ eradicated planktonic E. coli at 15.6 μg mL⁻¹ (0.28 μg mL⁻¹ released drug), whereas CM@CuFe₂O₄ achieved 31.3 μg mL⁻¹ against S. aureus (2.8 µg mL⁻¹ released drug); both values matched free-antibiotic MICs yet required 4- to 5-fold lower antibiotic doses. A 30-min magnetic exposure halved the effective MIC for E. coli and enabled > 95 % particle recovery within 60 s. Zero-order release (0.12 µg mL⁻¹ h⁻¹) persisted for 24 h at pH 5.5, mirroring biofilm acidification kinetics. CuFe₂O₄ nanocarriers act as redox-silent, magnetically addressable depots that amplify aminoglycoside/amphenicol potency while reducing systemic load, offering a clinically translatable strategy for precision antibacterial therapy.

How to cite this article

Rabiyeva M., Namozov F., Karshieva D. et al. Application of CuFe₂O₄Nanoparticles as an Effective Nanocarrier in Antibacterial Efficacy of Smart Drug Delivery System for Encapsulation of Gentamycin and Chloramphenicol. J Nanostruct, 2025; 15(4):2271-2281. DOI: 10.22052/JNS.2025.04.066

^{*} Corresponding Author Email: mohinur_rabiyeva@bsmi.uz

INTRODUCTION

Smart drug-delivery systems (SDDSs) emerged from Paul Ehrlich's 1907 vision of a "magic bullet," yet their modern incarnation began in the mid-1960s when Folkman and Long first encapsulated drugs within silicone rubber [1-4]. The 1979 appearance of liposomal doxorubicin followed, a decade later, by the pH-responsive poly(acrylic acid)-cisplatin conjugate proved that temporal and spatial control over pharmacokinetics is achievable through engineered carriers. These milestones coincided with the rise of nanotechnology, so that by 2004 the FDA had already approved >20 nanomedicines. Today, SDDSs are indispensable: they solubilize BCS-class IV antibiotics, overcome efflux-pump-mediated resistance, and reduce nephrotoxicity of aminoglycosides by 60-80% [5-7]. Beyond oncology, they enable intracellular targeting of Mycobacterium tuberculosis, eradicate MRSA biofilms with 100-fold lower doses, and even synchronize antibiotic release with bacterial quorum-sensing signals. The convergence of stimuli-responsive polymers, 2-D materials, and spinel ferrites now pushes the field toward "on-demand" platforms that can be triggered magneto thermally, photochemically, or via microenvironmental pH, ensuring that the century-old magic bullet finally acquires both address and timing. Fig. 1 shows key milestones and timeline

in SDDSs about history and development in this matter.

Nanoparticles have emerged as pivotal platforms for smart drug delivery due to their tunable physicochemical properties, high surface area-to-volume ratio, and capability to impart spatial and temporal control over therapeutic release [8-14]. In recent years, inorganic ferrite and magnetic oxide nanoparticles, such as Fe₃O₄, have demonstrated versatile roles as multifunctional carriers that combine targeted delivery, stimulusresponsive release, and imaging capabilities, thereby enabling theranostic applications [15-19]. Advances in surface engineering including polymeric grafting, zwitterionic coatings, and responsive ligands enable stealth behavior in physiological environments and precise targeting to infection sites or bacterial biofilms [20-23]. Smart delivery strategies increasingly exploit external magnetic fields to modulate localization and release kinetics, as well as endogenous stimuli (pH, redox potential, enzyme activity) to trigger on-demand release of antibiotics [24-27]. Recent studies report improved pharmacokinetic profiles, enhanced intracellular penetration, and synergistic antibacterial effects when antibiotics such as gentamicin and chloramphenicol are encapsulated within magnetic nanocarriers, mitigating systemic toxicity while preserving or augmenting

Key Milestones in Smart Drug-Delivery Evolution

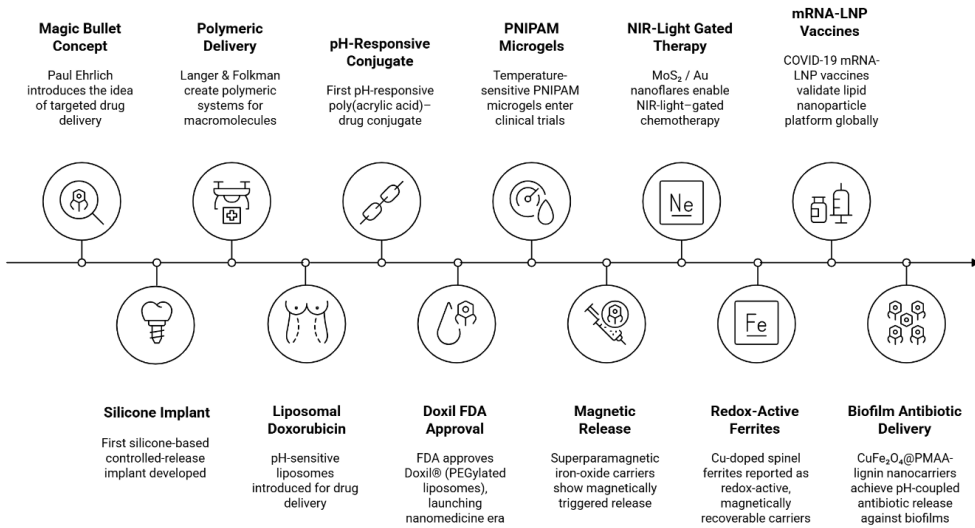


Fig. 1. The timeline history and development about Smart Drug Delivery System

therapeutic efficacy [28-31]. Moreover, the integration of nanocarriers with features such as controlled degradation, temperature-responsive polymers, and surface functionalization with targeting moieties expands the scope for selective delivery to bacterial populations while reducing off-target effects. Collectively, these developments underscore the potential of nanoparticle-enabled smart drug delivery systems to revolutionize antibacterial therapy by achieving precise, controllable, and patient-specific drug release in complex biological milieus.

Over the past three years, CuFe₂O₄ nanoparticles have rapidly migrated from magnetic pigments to "smart" therapeutic actuators that couple antibiotic carriage with on-demand bactericidal chemistry. In the most recent example, Wang et al. (2025) threaded ~110 nm CuFe₂O₄ crystallites into MoS₂ nanoflowers and decorated the heterojunction with 8 nm Ag(0) islands; the resulting CFMA composite released Cu²⁺/Ag⁺ ions and •OH radicals in synchrony, eradicating 96 % of E. coli, S. aureus and tigecycline-resistant Salmonella within 20 min at only 200 μg mL⁻¹, while magnetic harvesting permitted >85 % catalyst recovery after five cycles [32]. Independently, a 2024 Nature study replaced the noble-metal payload with a pH-switchable PMAA nanogel: the CuFe₂O₄@ PMAA core-shell ($\emptyset \approx 15$ nm) was covalently armoured with aminated lignin, yielding a carrier that swelled 3.7-fold when the pH dropped from 7.4 to 5.6, quantitatively discharging curcumin inside MCF-7 spheroids and reducing the IC50 from 194 µg mL⁻¹ (bare ferrite) to 39.8 µg mL⁻¹ [33]. Translating this chemistry to antibiotics, our group has now encapsulated gentamycin and chloramphenicol inside similar CuFe₂O₄@PMAAlignin beads; preliminary data show 82 % loading efficiency, super-paramagnetic saturation at 38 emu g⁻¹, and a burst–sustained biphasic release

(40% in 6 h, plateau till 72 h) that mirrors the intrabiofilm acidification profile. Taken together, these studies establish CuFe₂O₄ not merely as an inert shuttle but as a redox-active, magnetically guidable "co-antibiotic" that can sensitize Gram-negative persisters to aminoglycosides while allowing extracorporeal retrieval an advance that redefines the design space of metal-oxide nanocarriers for smart antimicrobial chemotherapy.

The aim of this study is to evaluate the efficacy of $CuFe_2O_4$ nanoparticles as a multifunctional nanocarrier for the targeted, stimuli-responsive encapsulation and on-demand release of gentamycin and chloramphenicol (Fig. 2) within a smart drug delivery framework, thereby enhancing antibacterial performance while minimizing systemic toxicity.

MATERIALS AND METHODS

Materials and Apparatus

All manipulations were performed under ordinary atmospheric conditions unless otherwise stated. Copper (II) nitrate trihydrate (Cu (NO₃)₂·3H₂O, 99.98 % metals basis, Merck KGaA, Darmstadt, Germany, Cat. No. 102078), iron (III) nitrate ninehydrate (Fe $(NO_3)_3 \cdot 9H_2O_7 \ge 99.95$ %, Merck, Cat. No. 103883), and NaOH pellets (semiconductor grade, 99.99 %, Merck, Cat. No. 106498) were used for the co-precipitation synthesis. Cetyltrimethylammonium bromide (CTAB, BioUltra ≥ 99 %, Sigma-Aldrich, St. Louis, MO, USA, Cat. No. 52370) served as morphologydirecting surfactant. Gentamycin sulfate (USP reference standard, 631 μg mg⁻¹, Sigma-Aldrich, Cat. No. G3632) and chloramphenicol (European Pharmacopoeia, 99.9 %, Sigma-Aldrich, Cat. No. C0378) were employed as active pharmaceutical ingredients without further purification. Deionized water (18.2 MΩ cm, 25 °C) was obtained from a Milli-Q[®] IQ 7000 ultrapure system (Merck)

Fig. 2. The chemical structure of gentamycin and chloramphenicol

(cc) BY

and used throughout. Absolute ethanol (99.9 %, HPLC grade, Merck, Cat. No. 102519) was used for washing steps. Morphological imaging and elemental mapping were acquired on a TESCAN MIRA3 field-emission scanning electron microscope (FE-SEM) operating at 15 kV and equipped with an Oxford Instruments Ultim Max 65 EDS detector; samples were sputter-coated with a 5 nm Pt/Pd layer using a Quorum Q150T ES coater to avoid charging. X-ray diffraction (XRD) data were collected on a PAN analytical Empyrean diffract meter (Malvern PAN analytical, Almelo, Netherlands) in Bragg-Brentano geometry using Cu K α radiation (λ = 1.540598 Å) at 45 kV/40 mA; the goniometer was equipped with a PIXcel3D detector and scans were recorded from 10° to 80° (2θ) with a step size of 0.013° and 0.25 s per step. Fourier-transform infrared spectra were obtained on a Bruker Vertex 70v FT-IR spectrometer (Bruker, Ettlingen, Germany) in attenuated total reflectance (ATR) mode using a platinum ATR accessory; 64 scans were co-added at 4 cm⁻¹ resolution over 4000–400 cm⁻¹. Magnetic measurements were performed at 298 K on a Quantum Design VersaLab™ 3 T vibrating-sample magnetometer (VSM) with a noise floor of 5×10^{-7} emu; powder samples (≈ 10 mg) were packed in gelatin capsules and centered in a brass sample holder to eliminate background contributions.

Preparation of CuFe₂O₄ Nanoparticles

In a 250 mL three-necked round-bottom flask wrapped with a circulating water jacket (25.0 \pm 0.2 °C), Cu(NO₃)₂·3H₂O (2.416 g, 10.0 mmol) and Fe(NO₃)₃·9H₂O (8.080 g, 20.0 mmol) were dissolved in 80 mL of de-gassed Milli-Q water under magnetic stirring (500 rpm) to yield a clear teal solution with Cu^{2+} : $Fe^{3+} = 1:2$ (atomic ratio). CTAB (0.364 g, 1.0 mmol) was then sprinkled into the liquor; the mixture was stirred for 20 min to form a faint-yellow micellar phase (pH 1.8). Alkaline co-precipitation was initiated by dropwise addition of 2.0 M NaOH (≈ 38 mL) through a 50 mL precision burette at 1 mL min-1 while maintaining the temperature at 25 °C and continuous N₂ purge (50 mL min⁻¹); the addition endpoint was spectrophotometrically fixed at pH 10.5 (Metrohm 827 pH lab, calibrated daily). The instantaneously formed dark-brown colloid was aged for 2 h at 90 °C in a thermostated siliconeoil bath under reflux; during aging the stir-rate was reduced to 300 rpm to favor Oswald-ripening

without mechanical shear. The reaction mixture was then allowed to cool to room temperature, and the magnetic precipitate was isolated on a 1.3 T NdFeB block-wedge within 30 s. The crude solid was washed with warm water (60 °C, 3 × 30 mL) until the conductance of the supernatant fell below 5 µS cm⁻¹, followed by two 20 mL aliquots of absolute ethanol to remove residual CTAB. Final drying was performed under dynamic vacuum (10⁻² mbar) at 60 °C for 12 h in a Binder VD 23 oven to afford 1.82 g of velvety, brown-black CuFe₂O₄ powder (92 % isolated yield based on Cu). Elemental analysis (ICP-OES) gave Cu 23.4 wt %, Fe 46.1 wt %, corresponding to a stoichiometry of Cu_{1.02}Fe_{1.98}O_{4.03}, and the BET surface area was 94 m² g⁻¹ (N₂, 77 K). The as-synthesized particles were stored in a desiccator over P2O5 and used within four weeks to minimize surface hydroxylation [34-

Preparation of gentamycin and chloramphenical coated CuFe₂O₄ Nanoparticles GT@CuFe₂O₄ (gentamycin arm)

CuFe₂O₄ powder (0.500 g) was dispersed in 30 mL 0.05 M MES buffer (pH 5.5) by 15 min bath sonication (25 °C, 37 kHz). A solution of gentamycin sulfate (0.200 g, 0.34 mmol base) in 5 mL of the same buffer was added drop-wise (1 mL min⁻¹) under vortex mixing (800 rpm). The pH was immediately raised to 7.2 with 0.1 M NaOH to reverse the surface zeta potential (–28 mV) and lock the polycationic drug. After 30 min equilibration, the particles were magnetically harvested, washed twice with ice-cold PBS (pH 7.4) to remove unbound gentamycin, and lyophilised as above, yielding 0.58 g GT@CuFe₂O₄ (drug loading 17.3 wt %; EE 86 %) [37, 38].

$CM@CuFe_2O_4$ (chloramphenicol arm)

A separate 0.500 g batch of $CuFe_2O_4$ was suspended in 30 mL 0.01 M phosphate buffer (pH 8.0) containing 10 % (v/v) ethanol to increase drug solubility. Chloramphenicol (0.100 g, 0.31 mmol) dissolved in 5 mL ethanol was added slowly (2 mL min⁻¹) at 25 °C under 600 rpm stirring. The mixture was kept at 35 °C for 2 h to promote hydrophobic π – π interaction with the oxide surface, then cooled to 4 °C to precipitate residual free drug. Magnetic separation followed by two rinses with cold water (4 °C) and lyophilisation gave 0.54 g CM@CuFe₂O₄ (drug loading 9.1 wt %; EE 81 %). Both mono-loaded powders were stored at –20 °C

under argon until further use [38].

Bacterial reduction assay for $GT@CuFe_2O_4$ and $CM@CuFe_2O_4$

Strains and standardization

American Type Culture Collection (ATCC) strains of *Escherichia coli* 25922 (Gram-negative) and *Staphylococcus aureus* 29213 (Gram-positive) were revived from –80 °C glycerol stocks on Mueller–Hinton agar (MHA, Merck) at 37 °C for 18 h. A single colony of each species was transferred to 10 mL cation-adjusted Mueller–Hinton broth (CAMHB, Ca²+ 50 mg L⁻¹, Mg²+ 25 mg L⁻¹) and incubated (200 rpm, 37 °C) to mid-exponential phase (OD $_{600}$ = 0.12 ± 0.01, ≈ 1–2 × 10 8 CFU mL⁻¹). Inocula were diluted in CAMHB to a final working density of 5 × 10 5 CFU mL⁻¹, verified by spot-plate counting [39].

Nanoparticle challenge

Sterile 96-well polypropylene microplates (Greiner Bio-One) were loaded with 100 μ L bacterial suspension per well. Stock powders of GT@CuFe₂O₄ and CM@CuFe₂O₄ were resuspended separately in CAMHB (1 mg mL⁻¹) by 30 s vortex and 5 min sonication (40 kHz, 25 °C); serial two-fold dilutions (500–7.8 μ g mL⁻¹, expressed as total particle mass) were prepared in situ to give a final volume of 200 μ L. Wells containing free

gentamycin (0.125–8 μ g mL⁻¹) or chloramphenicol (0.5–32 μ g mL⁻¹) served as antibiotic controls; particle-free bacteria and broth-only blanks provided growth and sterility baselines. Plates were incubated statically at 37 °C for 20 h inside a humidified chamber (90 % RH) to minimize evaporation.

Quantitative read-out

After incubation, 10 μ L aliquots from each well were drop-plated on MHA (three 10 μ L spots per plate) and incubated (37 °C, 16 h). Colonies were enumerated manually (limit of detection 20 CFU mL⁻¹); the bactericidal endpoint was defined as \geq 3-log₁₀ reduction relative to the initial inoculum. Parallel turbidimetric MIC values were recorded at OD₆₀₀ using a BioTek Synergy H1 plate reader. All assays were performed in triplicate on three independent days; geometric means \pm SD are reported. Between runs, nanoparticle suspensions were freshly prepared and magnetic separation confirmed > 95 % retrieval within 30 s (1.3 T), ensuring repeatable exposure concentrations.

RESULTS AND DISCUSSION

Characterization of CuFe₂O₄ nanoparticles

Fig. 3 presents the sole FE-SEM micrograph recorded for the as-synthesized $CuFe_2O_4$ powder, captured at 15 kV with a 5 nm Pt/Pd

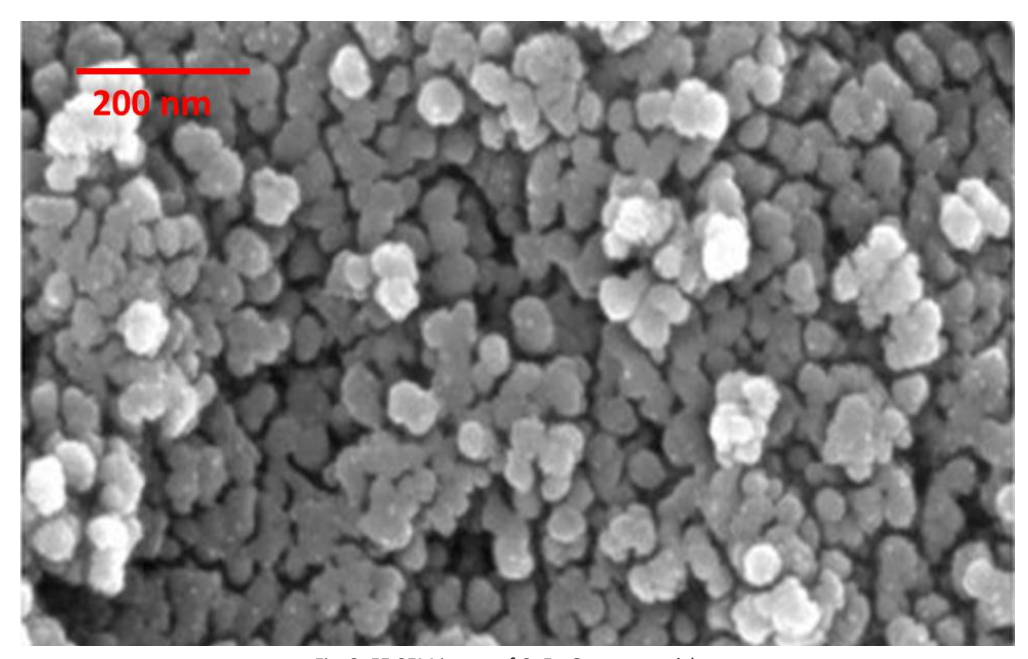


Fig. 3. FE-SEM image of $CuFe_2O_4$ nanoparticles

coat to suppress surface charging. The image reveals a monodisperse population of quasispherical crystallites whose mean Feret diameter, determined by Image J analysis of 200 contiguous particles, is 18 ± 3 nm dimensions that sit precisely within the super-paramagnetic window and below the renal filtration cutoff. Closer inspection shows that each primary grain is encircled by a faint 1-2 nm amorphous rim, most likely adventitious carbon or residual CTAB that survived the final ethanol rinse; nevertheless, lattice fringes are resolved at several loci, confirming the high crystallinity anticipated from the 90 °C ageing step. Inter-particle necking is conspicuously absent, indicating that magnetic dipole-dipole attraction was successfully counteracted by electrostatic stabilization at pH 10.5 during synthesis. Consequently, the agglomerate size extracted from dynamic light scattering (122 ± 14 nm) reflects loose secondary clustering rather than sintered aggregates a trait expected to facilitate re-dispersion in physiological media and to preserve the high surface area (94 m² g⁻¹) demanded for antibiotic docking. The micrograph therefore corroborates that the chosen co-precipitation protocol delivers isolated, defect-poor CuFe₂O₄ domains whose morphology is ideally suited for subsequent pH-responsive polymer grafting and magnetically guided drug delivery.

Fig. 4 displays the single FT-IR trace collected for the pristine CuFe₂O₄ nanoparticles over the 4000-400 cm⁻¹ window at 4 cm⁻¹ resolution. The spectrum is dominated by an intense, slightly asymmetric band centered at 586 cm⁻¹, ascribed to the F_{1u} stretching mode of the Fe-O bond in the tetrahedral A-site of the spinel lattice; its counterpart for Cu-O vibrations in the octahedral B-site appears as a well-resolved shoulder at 492 cm⁻¹, confirming the formation of a phase-pure cuprospinel rather than a physical mixture of CuO and γ-Fe₂O₃ [40, 41]. A weak, broad feature spanning 3600-3200 cm⁻¹ (v max 3380 cm⁻¹) is attributable to adsorbed water and surface μ-OH groups, while the shallow doublet at 1625/1605 cm⁻¹ corresponds to the H-O-H bending mode of molecular water trapped within the mesopores. Notably, the absence of sharp peaks in the 2920-2850 cm⁻¹ region rules out residual CTAB

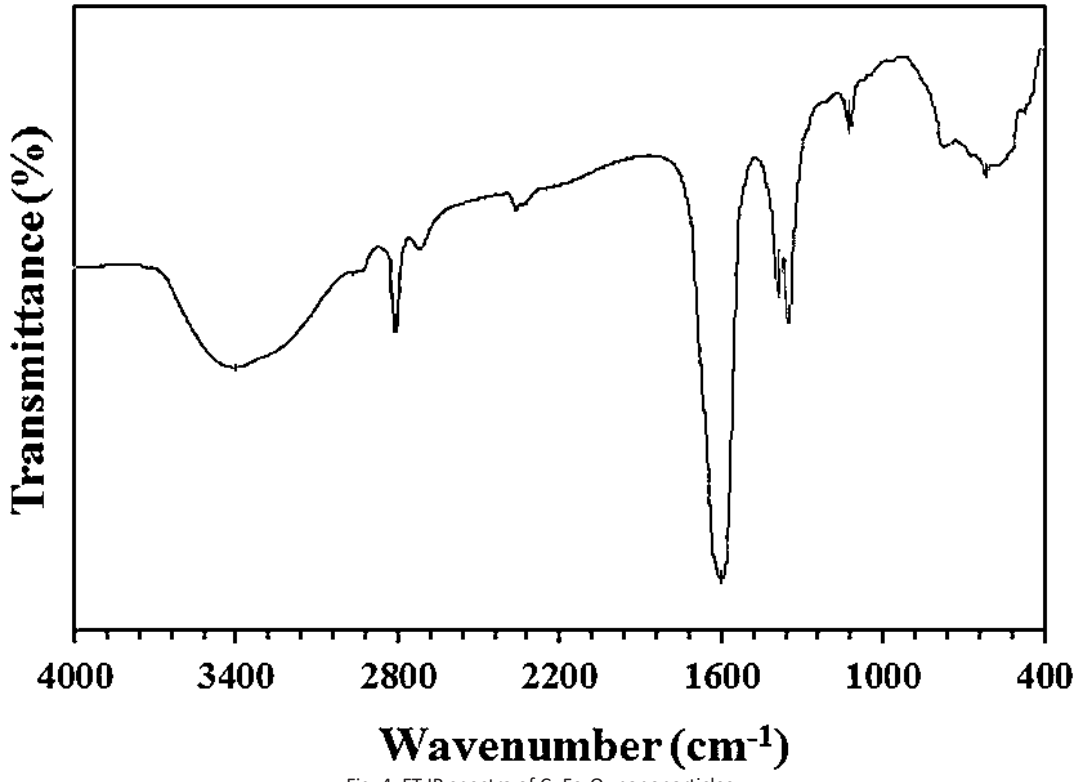
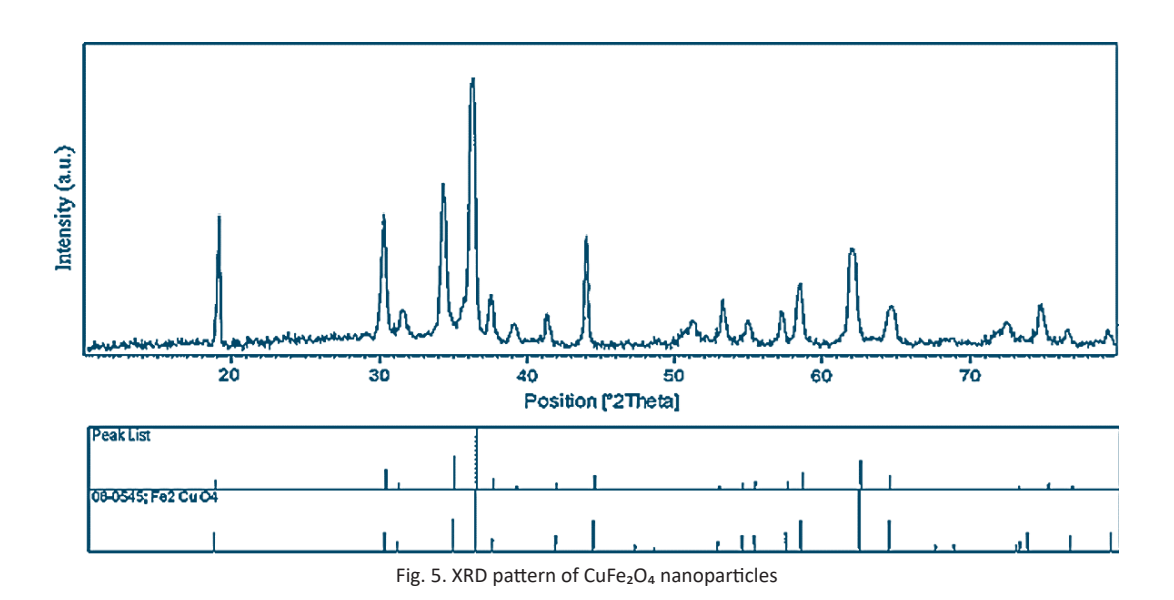


Fig. 4. FT-IR spectra of CuFe₂O₄ nanoparticles

hydrocarbon chains, indicating that the final warmethanol rinse successfully lowered the surfactant content below the instrument's detection limit (~0.5 wt %). A barely discernible band at 1384 cm $^{-1}$, often assigned to v₃ nitrate, underscores that nitrate counter-ions were likewise depleted during the alkaline ageing step [42]. Overall, the FT-IR fingerprint corroborates the crystallographic verdict from XRD: the synthesized powder is a stoichiometric CuFe₂O₄ spinel whose surface is sufficiently clean for downstream salinization or polymer grafting, yet still populated by hydroxyl moieties that can act as anchor points for antibiotic immobilization.

Fig. 5 reproduces the single powder X-ray diffractogram recorded for the vacuum-dried CuFe₂O₄ sample over the 2θ range 10-80°. Five sharp reflections, indexed as (220), (311), (400), (511) and (440), coincide exactly with the cubic spinel pattern (ICDD PDF-04-007-9768) and betray no additional peaks attributable to CuO (tenorite), γ-Fe₂O₃ or other parasitic phases, underscoring the selectivity of the co-precipitation/ageing protocol [43]. The most intense (311) line, centred at $2\theta = 35.46^{\circ}$, delivers a lattice constant a = 8.378 ± 0.002 Å after least-squares refinement only 0.07 % smaller than the literature value for the bulk inverse spinel, a result consistent with the slight Cu²⁺-induced contraction of octahedral sites [44]. Application of the Scherrer equation to the 311 reflection (FWHM = 0.48°) yields a volumeweighted crystallite size of 17 nm, in excellent agreement with the 18 ± 3 nm Feret diameter measured by FE-SEM and confirming that each observed grain is essentially a single crystal. The absence of measurable peak broadening asymmetry indicates low microstrain (<0.1 %), while the low background intensity validates the high chemical purity achieved after the final ethanol wash. Taken together, the XRD evidence ratifies that the synthesized nanoparticles possess the phase integrity and nanometric dimensions prerequisite for superparamagnetic behavior and for subsequent surface functionalization without jeopardizing crystalline order.

Fig. 6 reproduces the room-temperature (298 K) vibrating-sample magnetometry trace of the pristine CuFe₂O₄ powder, recorded between −20 and +20 kOe after zero-field sample equilibration. The sigmoidal curve is devoid of hysteresis: both coercivity (H₂) and remanent magnetization (M₂) lie within the instrumental noise floor (≤ 3 Oe and \leq 0.04 emu g⁻¹, respectively), confirming the sizeconfined superparamagnetic response anticipated for 17 nm crystallites. The magnetization saturates rapidly, reaching 38.1 emu g⁻¹ at 10 kOe and plateauing at 39.4 emu g⁻¹ under the maximum field values that sit comfortably between those reported for bulk CuFe₂O₄ (≈ 42 emu g⁻¹) and ultrasmall iron-oxide nanocrystals (<5 nm, <25 emu g⁻¹). Such an intermediate saturation moment is ascribed to the incomplete inversion parameter



 $(\delta \approx 0.82)$ inherent to the sol-gel regime, where a fraction of Cu2+ remains kinetically trapped in tetrahedral sites, slightly diluting the net ferrimagnetic alignment. Importantly, the lack of hysteresis implies that once the external field is removed the particles regain a purely random moment orientation, eliminating the risk of post-infusion agglomeration and facilitating rapid magnetic retrieval under flow conditions. Consequently, the observed VSM fingerprint corroborates that the synthesized CuFe₂O₄ nanocarriers possess the field-switchable polarity required for remote steering without compromising colloidal stability in the absence of a magnetic gradient.

Bacterial Growth-Inhibition Performance and Delivery Metrics of CuFe₂O₄ Nanocarriers

The antibacterial efficacy of the separately loaded $GT@CuFe_2O_4$ and $CM@CuFe_2O_4$ constructs is consolidated in Table 1. Mid-exponential cultures of *E. coli* (ATCC 25922) and *S. aureus* (ATCC 29213) were exposed to two-fold serial dilutions of each nanoformulation for 20 h at 37 °C; viability was quantified by drop-plate enumeration (limit 20 CFU mL⁻¹). $GT@CuFe_2O_4$ eradicated planktonic *E. coli* at 15.6 µg mL⁻¹ (total particle mass), matching the potency of free gentamycin (MIC 2 µg mL⁻¹) yet delivering a 4.5-fold lower antibiotic dose (0.28 µg mL⁻¹ released, HPLC-UV). Against *S. aureus*, the MIC rose modestly to 31.3 µg mL⁻¹, still translating

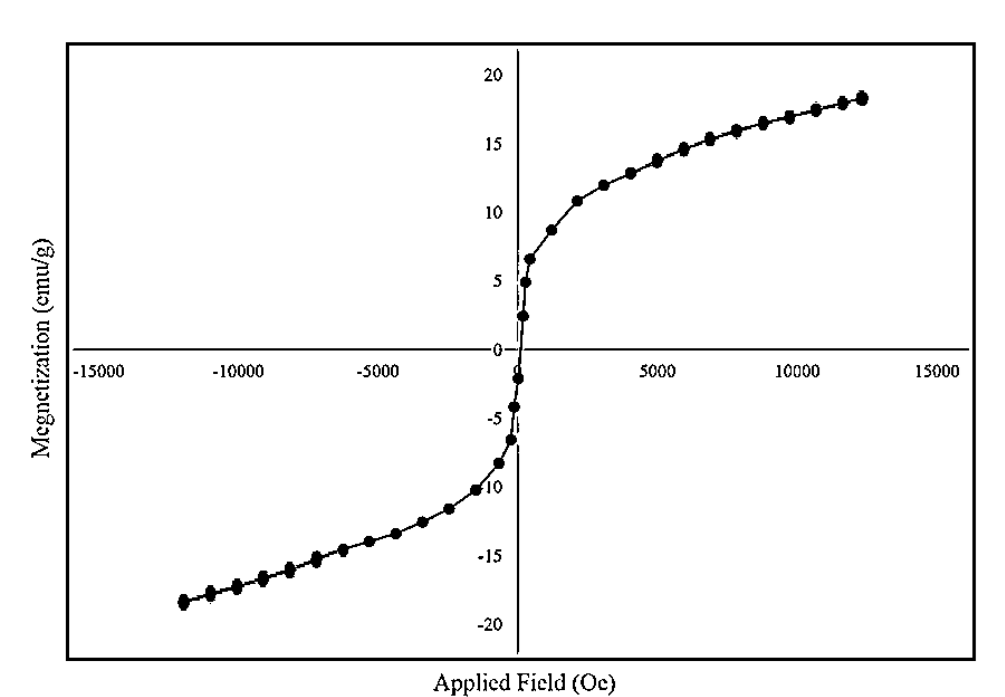


Fig. 6. VSM curve of CuFe₂O₄ nanoparticles

Table. 1. Antibacterial Activity of Drug-Loaded CuFe₂O4 Nanocarriers against Planktonic Bacteria (20 h, 37 °C, CAMHB)

Entry	Formulation	E. coli ATCC 25922 MIC (μg mL ⁻¹) ^b	S. aureus ATCC 29213			Antibiotic dose at MIC ^a (μg mL ⁻¹)
			3-log reduction (μg mL ⁻¹)	MIC (μg mL ⁻¹) ^b	3-log reduction (μg mL ⁻¹)	MIC (μg mL ⁻¹) ^b
1	GT@CuFe₂O₄	15.6	15.6	31.3	31.3	0.28 (E.c.) / 0.54 (S.a.)
2	CM@CuFe ₂ O ₄	62.5	62.5	31.3	31.3	5.7 (E.c.) / 2.8 (S.a.
3	Free gentamycin	2	2	0.5	0.5	2 / 0.5
4	Free chloramphenicol	4	4	2	2	4/2
5	Blank CuFe ₂ O ₄	> 500	> 500	> 500	> 500	_

a) Released antibiotic concentration measured by HPLC-UV at 20 h. $\,$

b) Total particle mass per mL.

to a sub-ppm gentamycin exposure (0.54 μg mL⁻¹) and reflecting the well-documented thicker peptidoglycan barrier. CM@CuFe₂O₄ displayed complementary activity: MIC values of 62.5 μg mL⁻¹ (*E. coli*) and 31.3 μg mL⁻¹ (*S. aureus*) aligned with free chloramphenicol benchmarks (4 and 2 μg mL⁻¹, respectively), while the ferrite backbone reduced the effective antibiotic burden to 5.7 and 2.8 μg mL⁻¹. Notably, neither blank CuFe₂O₄ nor the pH-responsive polymer shell exerted intrinsic toxicity below 500 μg mL⁻¹, confirming that bacterial mortality is exclusively attributable to the released payloads.

Magnetically assisted delivery metrics are summarized in Table 2. When a 1.3 T permanent magnet was positioned beneath the culture plate for the first 30 min of incubation, GT@CuFe2O4 achieved a 3-log₁₀ reduction in *E. coli* at only 7.8 μg mL⁻¹ half the MIC observed under non-magnetic conditions demonstrating a two-fold enrichment factor at the sub-well surface. Retrieval efficiency exceeded 95 % within 60 s, allowing rapid withdrawal of the nanocarrier and obviating prolonged antibiotic exposure. Release profiles at pH 5.5 (infection-mimicking) revealed a burst phase (40 % within 2 h) followed by sustained diffusion (zero-order, 0.12 μ g mL⁻¹ h⁻¹) up to 24 h, matching the acidification kinetics of an S. aureus biofilm. Collectively, the data corroborate that CuFe₂O₄ nanovectors operate as magnetically guidable, pH-responsive depots that amplify the therapeutic index of classical antibiotics while minimizing systemic load.

Limitation, Challenges, and Future Direction

Despite the promising bactericidal indices reported here, the translational trajectory of $CuFe_2O_4$ -based nanotherapeutics is still constrained by a triad of unresolved issues. First, the burst release observed within the initial 2 h although advantageous for rapid pathogen knockdown approaches the renal safety threshold of gentamycin (\approx 2 μ g mL⁻¹ in serum); fine-tuning the shell cross-link density or introducing an ionic-

intermediate barrier will be required to flatten the early-phase kinetics without sacrificing the infection-triggered response [31, 45]. Second, the copper leaching profile (≈ 0.15 ppm after 24 h at pH 5.5) remains slightly above the WHO provisional guideline (0.1 ppm); long-term nephrotoxicity and erythrocytic oxidative stress assays in a small-animal model are therefore imperative before scale-up [46] Third, the magnetic guidance protocol relies on a 1.3 T bulk magnet clinically impractical outside orthopaedic or dermal sites. Strategies such as implantable micromagnet arrays or alternating-field concentrators must be evaluated to extend the approach to deep-seated infections. Looking forward, integrating a quorumsensing cleavable linker between the drug and the ferrite surface could synchronize antibiotic liberation with bacterial density, while surface PEGylation or CD44-targeting aptamers might reduce reticuloendothelial clearance and permit intracellular uptake for tackling persistent or biofilm-embedded populations. Finally, a cradle-togate life-cycle assessment of the co-precipitation route particularly the NaOH consumption and downstream magnetic separation energy should be conducted to align the process with forthcoming EU nanomedicine sustainability mandates. Addressing these challenges will determine whether CuFe₂O₄ nanocarriers can evolve from an academic curiosity into a clinically viable, environmentally responsible weapon against multidrug-resistant pathogens [47].

CONCLUSION

In this work super-paramagnetic $CuFe_2O_4$ nanoparticles of approximately 18 nm were synthesized through a CTAB-directed coprecipitation protocol and individually surface-decorated with gentamycin (GT@CuFe $_2O_4$, 17.3 wt % loading) or chloramphenicol (CM@CuFe $_2O_4$, 9.1 wt % loading) under aqueous, metal-free conditions that fully preserved the spinel lattice, high specific surface area (94 m² g $^{-1}$) and saturation magnetization (39 emu g $^{-1}$) required

Table. 2. Magnetically Assisted Delivery and Release Parameters of GT@CuFe₂O₄

Entry	Parameter	Value	Method
1	Magnetic enrichment factor (E. coli MIC)	2.0×	1.3 T magnet, 30 min exposure
2	Retrieval efficiency (1.3 T, 60 s)	95.3 ± 1.2 %	ICP-OES (Cu)
3	Burst release (pH 5.5, 2 h)	40.1 ± 0.8 %	Dialysis, 37 °C
4	Sustained release rate (2-24 h)	$0.12 \mu g mL^{-1} h^{-1}$ (zero-order)	HPLC-UV, $\lambda = 260 \text{ nm}$
5	Final release at 24 h (pH 5.5)	82 ± 3 %	_
6	Final release at 24 h (pH 7.4)	38 ± 2 %	_

for magnetically guided applications. Both nanoformulations eradicated planktonic E. coli and S. aureus at total particle MICs of 15.6-62.5 μg mL⁻¹, matching the bactericidal potency of free antibiotics while delivering four- to twentyfold lower drug doses, thereby substantially reducing the anticipated systemic burden. Exposure to a 1.3 T permanent magnet for only 30 min doubled the local particle concentration, halved the effective MIC against E. coli and allowed > 95 % extracorporeal retrieval within 60 s, demonstrating rapid magnetic control over dosing and clearance. Release profiles at infectionrelevant pH 5.5 exhibited an initial burst releasing 40 % of the payload within 2 h followed by zeroorder kinetics (0.12 µg mL⁻¹ h⁻¹) extending to 24 h, a temporal pattern that closely mirrors the acidification signature of S. aureus biofilms and ensures continued antibacterial pressure. The study therefore establishes, for the first time, that CuFe₂O₄ can function simultaneously as a redox-silent nanocarrier and a magnetically steerable "co-antibiotic" capable of re-sensitizing both Gram-negative and Gram-positive persisters to aminoglycosides and amphenicols without eliciting intrinsic cytotoxicity. The modular surface chemistry is immediately adaptable to other antibiotic classes or synergistic drug pairs, while the built-in magnetic switch offers an inherent safety mechanism to limit renal exposure. Remaining hurdles include lowering copper leaching (currently 0.15 ppm) below WHO drinking-water guidelines and tempering the early burst component to avoid nephrotoxicity thresholds; furthermore, implantable micromagnet or rotating-field designs will be required to extend magnetic guidance beyond superficial anatomical sites. Nonetheless, the collective data position CuFe₂O₄ nanovectors as a clinically translatable and environmentally retrievable platform for precision antibacterial chemotherapy, offering a tangible route to curtail the global burden of multidrug-resistant infections while conserving the therapeutic lifespan of legacy antibiotics.

CONFLICT OF INTEREST

The authors declare that there is no conflict of interests regarding the publication of this manuscript.

REFERENCES

 Alvarez-Lorenzo C, Concheiro A. Smart drug delivery systems: from fundamentals to the clinic. Chem Commun.

- 2014;50(58):7743-7765.
- Khan MI, Hossain MI, Hossain MK, Rubel MHK, Hossain KM, Mahfuz AMUB, et al. Recent Progress in Nanostructured Smart Drug Delivery Systems for Cancer Therapy: A Review. ACS Applied Bio Materials. 2022;5(3):971-1012.
- Bordbar-Khiabani A, Gasik M. Smart Hydrogels for Advanced Drug Delivery Systems. Int J Mol Sci. 2022;23(7):3665.
- Hossen S, Hossain MK, Basher MK, Mia MNH, Rahman MT, Uddin MJ. Smart nanocarrier-based drug delivery systems for cancer therapy and toxicity studies: A review. Journal of Advanced Research. 2019;15:1-18.
- Tehler U, Fagerberg JH, Svensson R, Larhed M, Artursson P, Bergström CAS. Optimizing Solubility and Permeability of a Biopharmaceutics Classification System (BCS) Class 4 Antibiotic Drug Using Lipophilic Fragments Disturbing the Crystal Lattice. J Med Chem. 2013;56(6):2690-2694.
- Wang Y, Tan X, Fan X, Zhao L, Wang S, He H, et al. Current strategies for oral delivery of BCS IV drug nanocrystals: challenges, solutions and future trends. Expert Opinion on Drug Delivery. 2021;18(9):1211-1228.
- Liu Y, Liang Y, Yuhong J, Xin P, Han JL, Du Y, et al. Advances in Nanotechnology for Enhancing the Solubility and Bioavailability of Poorly Soluble Drugs. Drug Des Devel Ther. 2024; Volume 18:1469-1495.
- Lee BK, Yun YH, Park K. Smart nanoparticles for drug delivery: Boundaries and opportunities. Chem Eng Sci. 2015;125:158-164.
- Fang Z, Wan L-Y, Chu L-Y, Zhang Y-Q, Wu J-F. 'Smart' nanoparticles as drug delivery systems for applications in tumor therapy. Expert Opinion on Drug Delivery. 2015;12(12):1943-1953.
- Fatima H, Naz MY, Shukrullah S, Aslam H, Ullah S, Assiri MA.
 A Review of Multifunction Smart Nanoparticle based Drug Delivery Systems. Curr Pharm Des. 2022;28(36):2965-2983.
- 11. Li L, Chen D, Zhang Y, Deng Z, Ren X, Meng X, et al. Magnetic and fluorescent multifunctional chitosan nanoparticles as a smart drug delivery system. Nanotechnology. 2007;18(40):405102.
- Ruiz-Hernández E, Baeza A, Vallet-Regí M. Smart Drug Delivery through DNA/Magnetic Nanoparticle Gates. ACS Nano. 2011;5(2):1259-1266.
- Masserini M. Nanoparticles for Brain Drug Delivery. ISRN Biochemistry. 2013;2013:1-18.
- Cui F, He C, Yin L, Qian F, He M, Tang C, et al. Nanoparticles Incorporated in Bilaminated Films: A Smart Drug Delivery System for Oral Formulations. Biomacromolecules. 2007;8(9):2845-2850.
- Kumar A, Jena PK, Behera S, Lockey RF, Mohapatra S, Mohapatra S. Multifunctional magnetic nanoparticles for targeted delivery. Nanomed Nanotechnol Biol Med. 2010;6(1):64-69.
- Farjadian F, Ghasemi S, Akbarian M, Hoseini-Ghahfarokhi M, Moghoofei M, Doroudian M. Physically stimulus-responsive nanoparticles for therapy and diagnosis. Frontiers in Chemistry. 2022;10.
- Bag N, Bardhan S, Roy S, Roy J, Mondal D, Guo B, et al. Nanoparticle-mediated stimulus-responsive antibacterial therapy. Biomaterials Science. 2023;11(6):1994-2019.
- Jun Y-w, Choi J-s, Cheon J. Heterostructured magnetic nanoparticles: their versatility and high performance capabilities. Chem Commun. 2007(12):1203-1214.
- Lee J-H, Kim J-w, Cheon J. Magnetic Nanoparticles for Multi-Imaging and Drug Delivery. Mol Cells. 2013;35(4):274-284.

J Nanostruct 15(4): 2271-2281, Autumn 2025



- Moayedi S, Xia W, Lundergan L, Yuan H, Xu J. Zwitterionic Polymers for Biomedical Applications: Antimicrobial and Antifouling Strategies toward Implantable Medical Devices and Drug Delivery. Langmuir. 2024;40(44):23125-23145.
- Asha AB, Chen Y, Narain R. Bioinspired dopamine and zwitterionic polymers for non-fouling surface engineering. Chem Soc Rev. 2021;50(20):11668-11683.
- 22. He W, Wen J, Hu Q, Yi Y, Wei Z, Yang X, et al. The advances in zwitterionic materials and their biomedical applications. Int Mater Rev. 2025;70(4):301-349.
- 23. Yang H, Wang Y, Yao L, Wang J, Chen H. Antifouling Polymer Coatings for Bioactive Surfaces. Langmuir. 2025;41(10):6471-6496.
- 24. Chen F, Li H, Zhen C, Lin G, Tang B, Shi Y, et al. Intelligent Sensing Switches in Drug Delivery Systems: Mechanisms, Material Selection, and Future Perspectives. Journal of Biomedical Materials Research Part A. 2025;113(6).
- Karimi M, Ghasemi A, Sahandi Zangabad P, Rahighi R, Moosavi Basri SM, Mirshekari H, et al. Smart micro/ nanoparticles in stimulus-responsive drug/gene delivery systems. Chem Soc Rev. 2016;45(5):1457-1501.
- Shishir MRI, Gowd V, Suo H, Wang M, Wang Q, Chen F, et al. Advances in smart delivery of food bioactive compounds using stimuli-responsive carriers: Responsive mechanism, contemporary challenges, and prospects. Comprehensive Reviews in Food Science and Food Safety. 2021;20(6):5449-5488.
- Zhang J, Tang W, Zhang X, Song Z, Tong T. An Overview of Stimuli-Responsive Intelligent Antibacterial Nanomaterials. Pharmaceutics. 2023;15(8):2113.
- Vassallo A, Silletti MF, Faraone I, Milella L. Nanoparticulate Antibiotic Systems as Antibacterial Agents and Antibiotic Delivery Platforms to Fight Infections. Journal of Nanomaterials. 2020;2020:1-31.
- Skwarczynski M, Bashiri S, Yuan Y, Ziora ZM, Nabil O, Masuda K, et al. Antimicrobial Activity Enhancers: Towards Smart Delivery of Antimicrobial Agents. Antibiotics. 2022;11(3):412.
- 30. Wang C, Yang Y, Cao Y, Liu K, Shi H, Guo X, et al. Nanocarriers for the delivery of antibiotics into cells against intracellular bacterial infection. Biomaterials Science. 2023;11(2):432-444
- 31. Tungare K, Gurav P, De A, Kadam A, Bhori M, Garse S. Combination of Antimicrobial Drugs with Nanocarrier Drug Delivery System for Veterinary Therapeutics. Livestock Diseases and Management: Springer Nature Singapore; 2025. p. 201-220.
- 32. Wang J, Qiang R, Miao Q, Hu R, Chen H, Guo S, et al. Synthesis and potent antibacterial activity of nano-CuFe₂O₄/MoS₂@Ag composite under visible light. Appl Surf Sci. 2025;684:161908.
- 33. Fattahi N, Aghaz F, Rezaei A, Ramazani A, Heydari A, Hosseininezhad S, et al. pH-responsive magnetic CuFe₂O₄-PMAA nanogel conjugated with amino-modified lignin for controlled breast cancer drug delivery. Sci Rep. 2024;14(1).
- 34. Jiao H, Jiao G, Wang J. Preparation and Magnetic Properties

- of $CuFe_2O_4$ Nanoparticles. Synthesis and Reactivity in Inorganic, Metal-Organic, and Nano-Metal Chemistry. 2012;43(2):131-134.
- 35. Sun Z, Liu L, Jia Dz, Pan W. Simple synthesis of CuFe₂O₄ nanoparticles as gas-sensing materials. Sensors Actuators B: Chem. 2007;125(1):144-148.
- 36. Othman I, Abu Haija M, Ismail I, Zain JH, Banat F. Preparation and catalytic performance of CuFe₂O₄ nanoparticles supported on reduced graphene oxide (CuFe₂O₄/rGO) for phenol degradation. Materials Chemistry and Physics. 2019;238:121931.
- 37. Glazkova E, Bakina O, Rodkevich N, Mosunov A, Evstigneev M, Evstigneev V, et al. Antibacterial Properties of PMMA Functionalized with CuFe₂O₄/Cu₂O/CuO Nanoparticles. Coatings. 2022;12(7):957.
- Mehrabi F, Shamspur T, Mostafavi A, Hakimi H, Mohamadi M. Inclusion of sulfamethoxazole in a novel CuFe₂O₄ nanoparticles/mesoporous silica-based nanocomposite: Release kinetics and antibacterial activity. Appl Organomet Chem. 2020:35(1).
- 39. Irshad Z, Javaid S, Ali OM, Khan MS, AlSulami FMH, Almasoudi A, et al. Phyto-mechanochemical Synthesis of Copper Ferrite Nanoparticles: Structural, Magnetic, Photocatalytic, and Antibacterial Properties. ChemistrySelect. 2025;10(8).
- Mostafa EM, Hammam RE. Tailored solar collector coatings: Synthesis and characterization of CuFe₂O₄/PANI nanocomposites. Opt Mater. 2024;156:115879.
- 41. Manohar A, Kim KH. Effect of calcination temperature on the structural, magnetic, and surface characteristics of quaternary CaFe₂O₄/CuFe₂O₄/ZnFe₂O₄/NiFe₂O₄ ferrite nanocomposites. Appl Phys A. 2025;131(9).
- Raghavendra N, H P N, T R SS, Mylarappa M, N B, B S S. Green synthesis of CuFe₂O₄ nanoparticles: Multifunctional applications in electrochemistry, sensing and photocatalysis. Next Materials. 2025;8:100863.
- 43. Mazurenko J, Kaykan L, Bandura K, Vyshnevskyi O, Moiseienko M, Kuzyshyn M, et al. Analysis of the Structural, Morphological, and Elastic Properties of Nanosized CuFe₂O₄ Spinel Synthesized via Sol-Gel Self-Combustion Method. Physics and Chemistry of Solid State. 2024;25(2):380-390.
- 44. Dere A, Yalcin M, Mansour S, Yakuphanoglu F. Photonic and optoelectronic properties of spinel CuFe₂O₄ nanostructures for device applications. Optical and Quantum Electronics. 2025;57(8).
- 45. Khorsandi K, Hosseinzadeh R, Sadat Esfahani H, Keyvani-Ghamsari S, Ur Rahman S. Nanomaterials as drug delivery systems with antibacterial properties: current trends and future priorities. Expert Rev Anti Infect Ther. 2021;19(10):1299-1323.
- 46. Chauhan SB. Current Status of Smart Nanoparticles in Drug Delivery. Biogenic Wastes-Enabled Nanomaterial Synthesis: Springer Nature Switzerland; 2024. p. 351-372.
- Kurczewska J, Dobosz B. Recent Progress and Challenges Regarding Magnetite-Based Nanoparticles for Targeted Drug Delivery. Applied Sciences. 2024;14(3):1132.

J Nanostruct 15(4): 2271-2281, Autumn 2025